



Deliverable 1.2.1

Name: Definition of the Reference Wind Turbine–Analysis of Rotor Design Parameters

May 2013

Agreement n.:	308974
Duration	60 months from 1 st November 2012
Co-ordinator:	Mr Peter Hjuler Jensen
Supported by:	EU 7 th Framework Programme

Support by:



PROPRIETARY RIGHTS STATEMENT

This document contains information, which is proprietary to the "INN WIND.EU" Consortium. Neither this document nor the information contained herein shall be used, duplicated or communicated by any means to any third party, in whole or in parts, except with prior written consent of the "INN WIND.EU" consortium.

Document information

Document Name:	Definition of the Reference Wind Turbine – Analysis of Rotor Design Parameters
Document Number:	Deliverable D1.2.1 – CRES Contribution
Author:	P.K. Chaviaropoulos , D. Chortis and D. Lekou (CRES)
Review:	Christian Bak (DTU) – aerodynamic part
Date:	May 2013
WP:	WP1: Conceptual Design
Task:	Task 1.2: Assessment of Innovation at the Subsystem Level

TABLE OF CONTENTS

TABLE OF CONTENTS	4
LIST OF FIGURES & TABLES	5
INTRODUCTION	6
Scope and Objectives	6
REVIEW OF THE RWT AERODYNAMIC DATA	7
Blade Planform Characteristics	7
Airfoils	8
Rotor Operating Conditions	10
RWT ROTOR PERFORMANCE	11
Performance at the Design Point	11
Overall Rotor Performance	14
SENSITIVITY ANALYSIS	16
Pitch Schedule	16
Blade Chord	17
Airfoils' Performance	18
STRUCTURAL PARAMETRIC ANALYSIS	20
Blade structural properties	20
Model Verification	23
Effect of mass increase on blade dynamic response	25
Effect of stiffness increase on blade dynamic response	27
CONCLUSIONS	29
REFERENCES	30

LIST OF FIGURES & TABLES

Figure 1. Blade planform characteristics – chord, twist and relative thickness radial distribution –	8
Figure 2. Lift and drag coefficient vs angle of attack. FFA family profiles along with the sectional C_L and C_D derived through interpolation based on the relative thickness	9
Figure 3. Rotational speed and pitch schedule as a function of the wind speed	10
Figure 4. Pressure, thrust coefficients and axial induction factor (α) distributions along the blade at design conditions ($\lambda = 7.5$)	11
Figure 5. Normalized radial distributions of the non-dimensional lift and the flow angle at design conditions ($\lambda = 7.5$)	12
Figure 6. Normalized radial distributions of the lift over drag and the corresponding angle of attack at design conditions ($\lambda = 7.5$)	13
Figure 7. Performance plot of the blade sections derived through interpolation based on the relative thickness	13
Figure 8. Pressure, thrust, torque (C_Q) and root bending moment coefficients (C_{RBM}) versus the wind speed	14
Figure 9. Dimensional thrust, torque and root bending moment versus the wind speed	15
Figure 10. Power curve sensitivity to pitch angle	16
Figure 11. Power and thrust coefficients sensitivity to blade chord	17
Figure 12. Torque, thrust and blade root bending moment sensitivity to blade chord	17
Figure 13. Power and thrust coefficients sensitivity to airfoils' drag	18
Figure 14. Torque, thrust and blade root bending moment sensitivity to airfoils' drag	19
Figure 15. First frequency in flap direction for various blades with respect blade length	20
Figure 16. First frequency in edge direction for various blades with respect to blade length	21
Figure 17. Stiffness distribution along the blade in flapwise direction for various blade sizes	22
Figure 18. Stiffness distribution along the blade in edgewise direction for various blade sizes	22
Figure 19. Normalized mass distribution along the blade for various blade sizes	23
Figure 20. First blade eigenmode (0.634Hz) – straight blade model	24
Figure 21. Second blade eigenmode (0.966Hz) – straight blade model	25
Figure 22. Blade mass increase: (a) Total blade mass; (b) Mass distribution along blade's span	26
Figure 23. First three natural frequencies of the blade model for increasing mass values	26
Figure 24. Variation of blade's 1 st flapwise natural frequency	27
Figure 25. Variation of blade's 2 nd flapwise natural frequency	28
Figure 26. Variation of blade's 1 st edgewise natural frequency	28
Table 1. Reference values of the 10MW InnWind blade	24

INTRODUCTION

Scope and Objectives

The present document is part of CRES' contribution to Deliverable 1.21 titled "Definition of the Reference Wind Turbine (RWT)". It comprises:

- An aerodynamic analysis of the RWT rotor including a review of the data offered by DTU [1]. The intention of this exercise is to validate the distributed dataset and verify the reported RWT aerodynamic performance using a second aerodynamic model. This is, still, a BEM-type model developed at CRES.
- A sensitivity analysis of the RWT aerodynamic performance in terms of critical aerodynamic design parameters and selections made.
- A parametric structural analysis where the effect of mass and stiffness changes of the blade structure on the dynamic response of the blade is investigated.

Apart from cross-checking data and performance figures the main objective of this work is to identify and highlight important design aspects that the Innwind.EU consortium should take advantage of in developing innovative aerodynamic concepts in WP2 (Lightweight Rotor).

REVIEW OF THE RWT AERODYNAMIC DATA

The model used by CRES in this work is an in-house BEM [2], [3] with the following specifications:

- The model reads the blade data at nodal points from r_{\min} (=0) to r_{\max} (= R, the rotor radius) but solves the BEM equations at mid-nodes where it also calculates the local aerodynamic coefficients.
- The BEM equations are solved all over the hub and blade span, including the non-lifting or low-lifting inboard sections.
 - Data interpolation and integration is based on linear schemes.
- Linear interpolation, based on the relative thickness, is used for extracting the lift and drag sectional data from the given airfoils' database. Here, the 3D-corrected FFA-W3-xxx data are used in all cases.
- The C_t (local thrust coefficient) - a (axial induction) formula in the BEM model is the following:

$$C_t = \begin{cases} 4a(1-a)F & \text{when } 0 \leq a \leq 0.4 \\ (.8a + .64)F & \text{when } 0.4 < a \end{cases} \quad (1)$$

where F is the tip-correction given by the formula

$$F = \frac{2}{\pi} \cos^{-1} \left[\exp \left\{ -\frac{(1-x)B\lambda}{2(1-a)} \right\} \right] \quad (2)$$

B is the number of blades, $\lambda = \omega R/V$ is the tip-speed ratio and $x = r/R$ is the radius fraction.

Blade Planform Characteristics

The blade planform data are provided at 41 radial stations. The rotor radius is $R=89.166$ m. The data comprise the chord length, the twist angle and the relative thickness of the relevant blade section. All three radial distributions are shown in figure 1. The radial discretization is also presented on the chord plot. It can be seen that the aerodynamic part of the blade starts at 30 meters from the rotation axis. Nearly the outer 50 meters of the blade are having the same relative thickness equal to 24.1%. This is a rather high value which affects the minimum drag of the blade section and therefore reduces the C_{P_MAX} of the rotor. Nevertheless, the drag penalty due to the higher airfoil thickness is partially compensated from the high Reynolds number of this large, high speed (rated tip-speed 90 m/s), rotor.

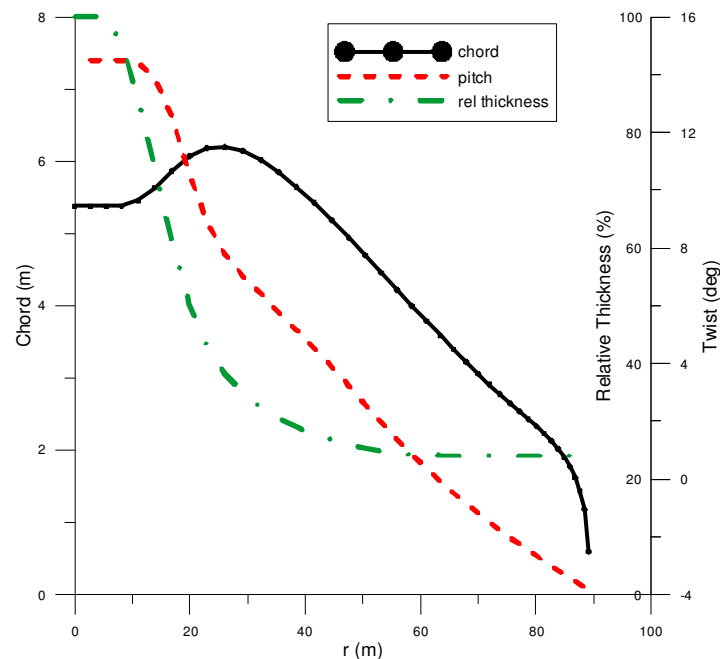


Figure 1. Blade planform characteristics – chord, twist and relative thickness radial distribution

Airfoils

Figure 2 presents plots of the lift C_L and drag C_D coefficients versus the angle of attack for the airfoils of the RWT rotor. There are five primary profiles of different thickness (24.1%, 30.1%, 36%, 48% and 60%) comprising the adopted FFA-W3 family. A typical cylindrical section is also given (corresponding to relative thickness 100%). The aerodynamic coefficients are provided for each profile over the angle of attack range [-180, +180] (degs) for a single Reynolds number representative of the operating conditions at the corresponding radial station. For instance, the FFA-W3-241 characteristics are given for $Re=12$ mil, a representative number for the near-design-point operating conditions at the outer part of the blade. It is known that value of the Reynolds number is affecting the maximum lift and, especially, the minimum drag. For pitch – variable speed rotors, as the one considered here, the Re influence on minimum drag is most important since its level is directly linked to C_{P_MAX} (which is obtained at the design conditions). Nevertheless, the sensitivity of the airfoil polars to small Reynolds number variations is rather low at the high Re numbers considered here.

DTU [1] provides two sets of C_L and C_D (but also pitching moment C_M) tabular data. The first set corresponds to normal 2-D profile data while the second includes corrections for 3-D and rotational effects. Here we shall only consider the second dataset. The applied corrections are clearly seen in the lift plot of figure 2. The high lift values (>2) of the inboard profiles (FFA-W3-480 and FFA-W3-600) at a.o.a above 15 degrees are attributed to the Coriolis pumping effect. Going outboards the blade is dominated by the FFA-W3-241 profile which retains its 2-D behaviour.

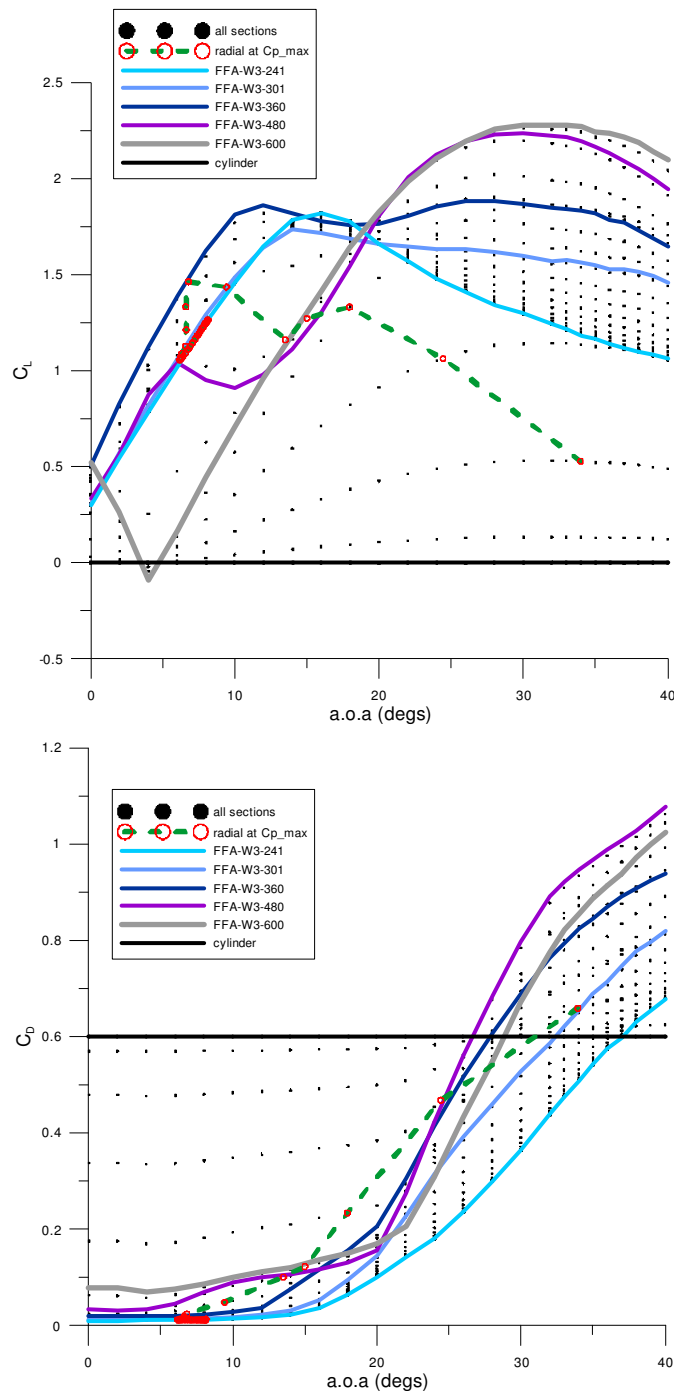


Figure 2. Lift and drag coefficient vs angle of attack. FFA family profiles along with the sectional C_L and C_D derived through interpolation based on the relative thickness

Using the FFA-W3 family and the cylindrical section we obtain the relevant C_L and C_D tables at any radial position using linear interpolation based on the relative thickness (following figure 1). The C_L variation of all 41 blade sections over the incidence range 0 to 40 degs is shown on figure 2 labelled as “all sections”. This “all sections” cloud fills-in the area between the different profiles, converging to the FFA-W3-241 lift curve as $r \rightarrow R$.

On the lift and drag plots of figure 2 we also present the “operating point” of all the airfoils at rotor design conditions (corresponding to $\lambda = 7.5$). Clearly, as r increases, the red-dots corresponding to the radial distribution of the design C_L and C_D converge towards the FFA-W3-241 polars travelling, however, along them. This indicates that the outer part of the blade is not operating at its maximum lift over drag point (maximum performance). Nevertheless, the minimum-drag pocket of the FFA-W3-241 profile is wide enough to prevent a significant C_{P_MAX} drop for this reason. On the other hand, a travelling operating point may render a less-deep C_{P_MAX} optimum, in benefit of the near-design conditions. We shall further discuss this issue below.

Rotor Operating Conditions

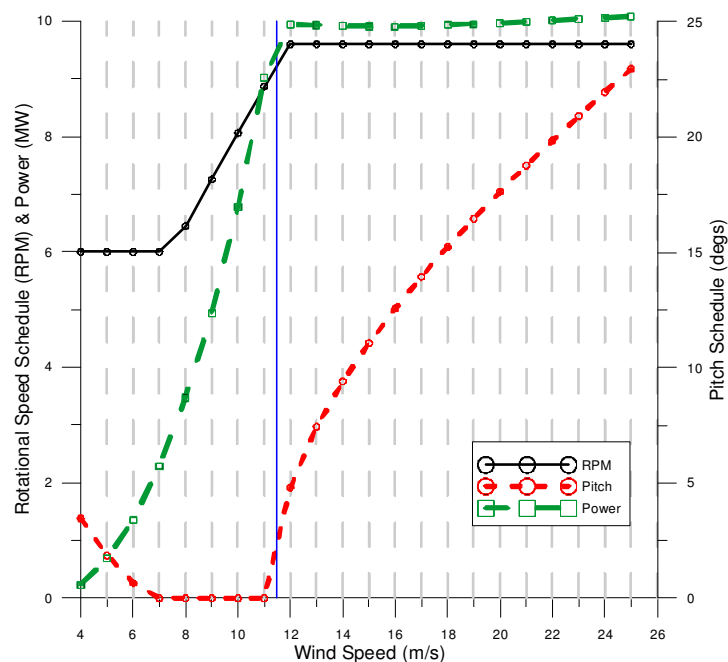


Figure 3. Rotational speed and pitch schedule as a function of the wind speed

As already mentioned the RWT rotor has been designed for Tip-Speed-Ratio $\lambda = 7.5$. The rotational speed schedule respects this optimum λ in the N_{MIN} - N_{MAX} range [6 – 9.6 RPM] corresponding to the wind speed range 7.5 m/s to 11.9 m/s. Below 7.5 m/s and above the cut-in wind speed (4 m/s) the turbine rotates with $N=6$ RPM, facilitated at its start-up region with some limited pitch action. Pitching is also activated above 11 m/s to keep the produced power to its rated level of 10 MW. Limited pitching action is also present in the transitional region 11 m/s to 11.5 m/s, the latter being the rated wind speed of the RWT. This is a rather non-conventional combination of pitch / variable-speed combination in this range, attributed to the rather low design TSR for a tip-speed of 90 m/s. The mechanical to electrical efficiency of the power train is assumed constant at all loads (partial and full), having the value $\eta = 0.94$.

The rotational speed / pitching schedule of the RWT used here were provided by DTU [4] with a wind-speed resolution of 1 m/s. Pitch setting and rotational speed are plotted in figure 3 along with the resulting power curve. It should be noted that the above-rated part of the power curve is very sensitive to the pitch angle. To obtain a flat power curve above 11.5 m/s we had to reduce the initial pitch setting by 1% at all speeds.

RWT ROTOR PERFORMANCE

Performance at the Design Point

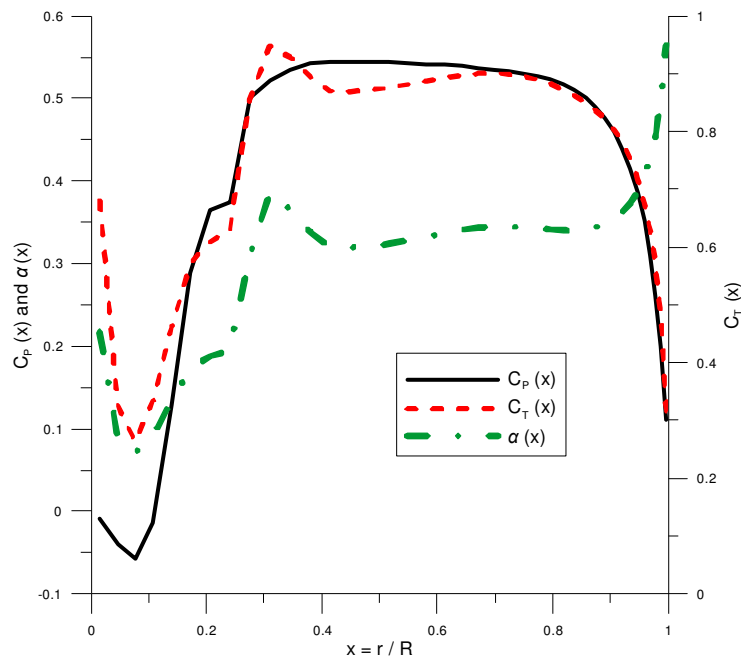


Figure 4. Pressure, thrust coefficients and axial induction factor (α) distributions along the blade at design conditions ($\lambda = 7.5$)

Figure 4 presents radial distributions of the local pressure, thrust coefficient and axial induction factor at rotor design conditions ($\lambda = 7.5$). It can be seen that at the aerodynamic part of the blade ($30\% < x < 85\%$) all three distributions are almost flat with α approaching its theoretical optimum value 0.33. The local power coefficient exceeds 0.5. For $x > 85\%$ there are severe tip effects that drive both C_p and C_t towards zero, as expected. For $x < 30\%$ there is a drop of all three coefficients, C_p taking negative values at the first 10% of the blade. The BEM solution in the area $0\% < x < 30\%$ is associated with significant uncertainties that are model- and data- dependent. The overall rotor C_p at $\lambda = 7.5$ is calculated at 0.473. A similar value is obtained by DTU when BEM modeling is used, while a higher value of 0.486 obtained with CFD modeling (EllipSys 3D code). According to the DTU colleagues this is attributed to the inboard performance of the blade, properly captured by the CFD model and to a lesser extent by the 3D and rotational corrections employed in BEM simulations. In any case, the blade root region requires further investigation and might be an investigation area for rotor performance improvement.

Figure 5 presents the radial distribution at design conditions ($\lambda = 7.5$) of the non-dimensional lift, defined as

$$L(\lambda, x) = \frac{c(\lambda, x)c_L}{R} \quad (3)$$

and the flow angle φ

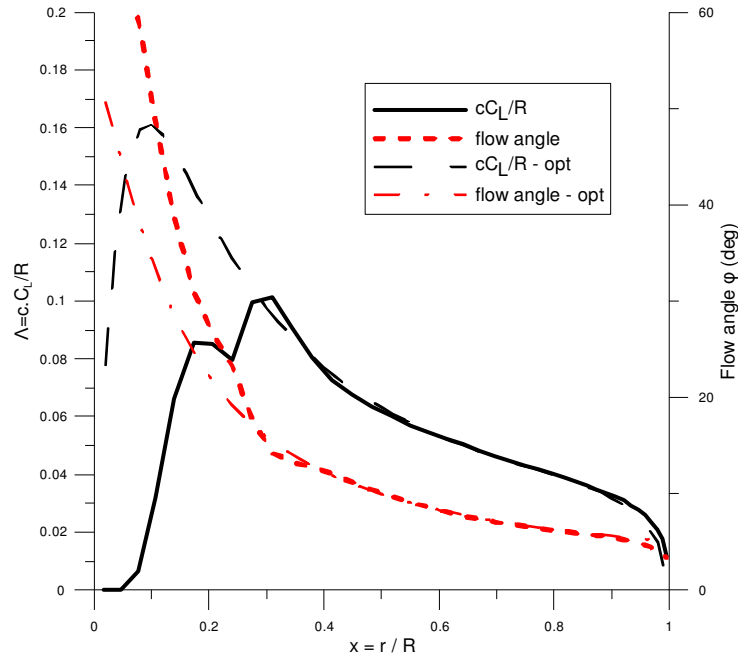


Figure 5. Normalized radial distributions of the non-dimensional lift and the flow angle at design conditions ($\lambda = 7.5$)

On the same figure we present (denoted as -opt) the optimal Λ and φ distributions following equations (4), (5) and (6) given in ref [5]

$$\Lambda(\lambda, x) = \frac{8\pi a(1-a)}{B\lambda(1+a')\sqrt{(1-a)^2 + \lambda^2 x^2(1+a')^2}} \frac{F}{\left[1 + \frac{(1-a)}{k\lambda x(1+a')}\right]} \quad (4)$$

$$\tan \varphi = \frac{(1-a)}{\lambda x(1+a')} \quad (5)$$

with the peripheral induction a' calculated from

$$a' = \frac{\sqrt{(k\lambda x)^2 + 2k\lambda x - 4ak[\lambda x - k(1-a) + 1]} - (k\lambda x + 1)}{2k\lambda x} \quad (6)$$

Equations (4) to (6) have been applied with $B=3$ (the number of blades), $\lambda = 7.5$, $k = 100$ (the airfoil performance, defined as the maximum of its C_L/C_D) and $\alpha = 0.33$. The selection of k value is compatible with the maximum performance of FFA-W3-241, dominating the aerodynamic part of the blade. From this comparison it is seen that the RWT blade is exactly matching the theoretical optimal distributions in the x -range 35% to 95%. Obviously, the deviation in the inner part of the blade ($x < 35\%$) is due to the need for having a realistic load carrying design of higher relative thickness and logical chord length. The Λ plot in the range $20\% < x < 35\%$ is pretty irregular. This irregularity is reflected to the aerodynamic coefficients of figure (4).

Elaborating on airfoil performance we present in figure 6 the radial distribution of C_L/C_D along with the corresponding angle of attack calculated by the BEM code, against the distributions of $k = \max(C_L/C_D)$ and its angle of attack of the airfoil placed at that x . To achieve maximum rotor performance at the design point these distributions, at least in the aerodynamic part of the blade, should exactly match each other, which is not the case here.

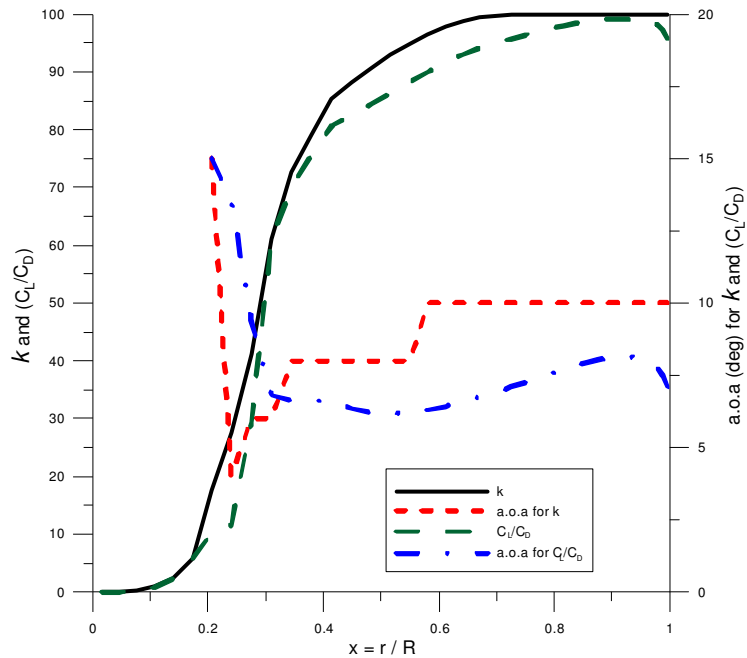


Figure 6. Normalized radial distributions of the lift over drag and the corresponding angle of attack at design conditions ($\lambda = 7.5$)

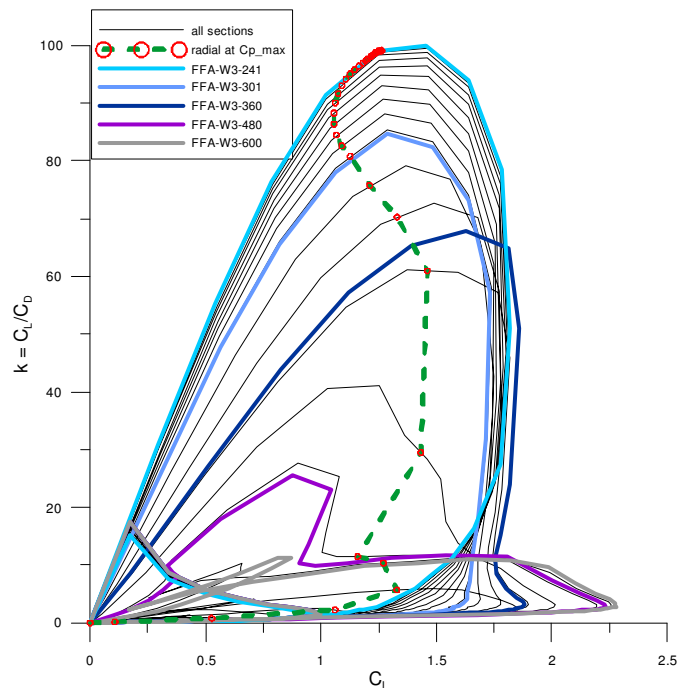


Figure 7. Performance plot of the blade sections derived through interpolation based on the relative thickness

Notably, the differences in the plot of angles of attack are relatively larger than the differences in airfoil performance, indicating that the airfoils used are having rather flat

characteristics around their maximum performance, which is important for near-design operation.

The above findings are better illustrated in figure 7 where (C_L/C_D) versus C_L plots are presented at all the blade sections. It is seen that the red-dots, indicating the actual performance of every blade section, are not coinciding with the sections' maximum performance point. This is true for the entire aerodynamic part of the blade. Staying close but not exactly on the maximum performance point of the individual blade sections has a penalty on C_{P_MAX} . On the other hand this may smoothen near-design operation. Similar remarks have been made earlier discussing figures 2 and 6. It is worth noting, however, that although the RWT blade has been designed for maximum C_P , other off design constraints (like reduced loading at stand-still) have been also satisfied, preventing the full matching of design (C_L/C_D) with $\max(C_L/C_D)$.

Overall Rotor Performance

We shall elaborate on rotor power (P), thrust (T), torque (Q) and thrust bending moment $M(r)$ (at a given radial position) and the relevant non-dimensional coefficients C_{xxx} defined through the following relations:

$$P = \frac{1}{2} \rho \pi R^2 V^3 C_P \quad (7)$$

$$T = \frac{1}{2} \rho \pi R^2 V^2 C_T \quad (8)$$

$$Q = \frac{1}{2} \rho \pi R^3 V^2 C_Q \quad (9)$$

$$M(r) = \frac{1}{2} \rho \pi R^3 V^2 C_{BM(r)} \quad (10)$$

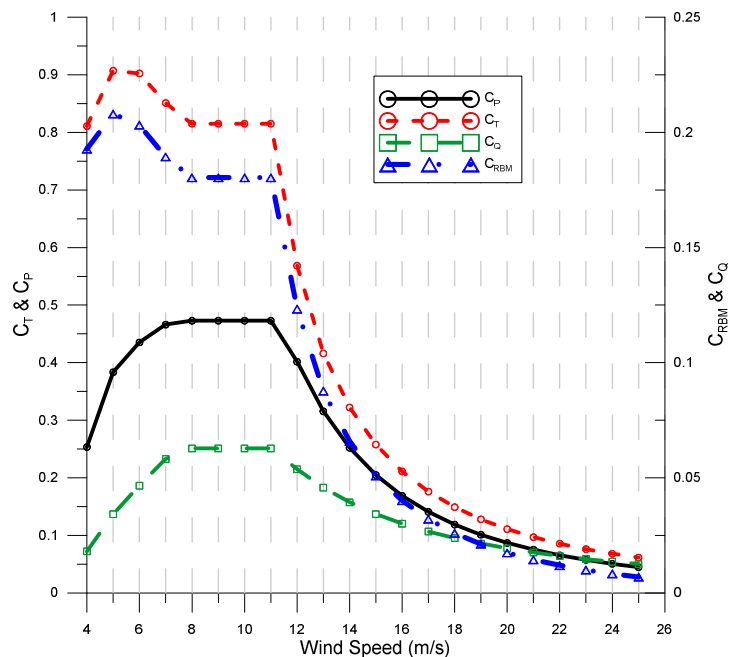


Figure 8. Pressure, thrust, torque (C_Q) and root bending moment coefficients (C_{RBM}) versus the wind speed

Figure 8 presents the variation of above four coefficients with the wind speed, ranging from its cut-in to its cut-out value. The coefficients are retain constant values in the variable speed region and are adjusted to the desired power level after rated wind speed. The thrust and bending moment coefficients are taking their largest values at very low

wind speeds where the corresponding loads are negligible. As already mentioned the calculated value of C_{P_MAX} is 0.473.

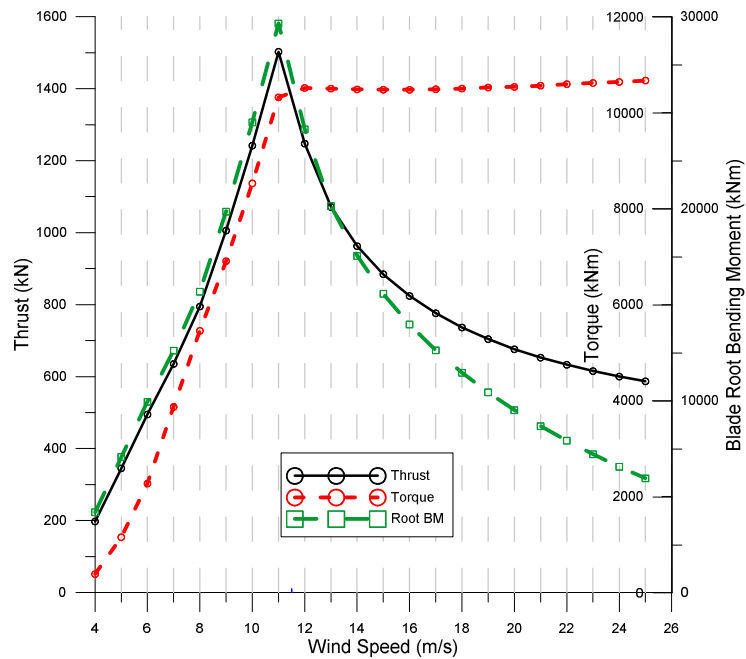


Figure 9. Dimensional thrust, torque and root bending moment versus the wind speed

The variation of rotor thrust, torque and thrust bending moment at blade root over the wind speed operating regime is presented in figure 9. As expected for pitch-variable speed designs, the maximum values of all three loads are obtained at rated wind speed. The maximum thrust is close to 1 500 kN while the corresponding root bending moment (at $r=0$) is close to 30 000 kNm. The maximum torque value is around 10600 kNm.

SENSITIVITY ANALYSIS

In this section we shall investigate:

- The sensitivity of the power production to the collective pitch angle at post-rated conditions
- The sensitivity of power production and rotor loading to blade solidity at below-rated conditions
- The sensitivity of power production and rotor loading to airfoils' performance characteristics at below-rated conditions

In each case the parameter investigated have been varied by a $\pm \Delta$ around its initial value by multiplying the pitch schedule, the chord radial distribution and the drag coefficient of all airfoils with $(1 \pm \Delta)$.

Pitch Schedule

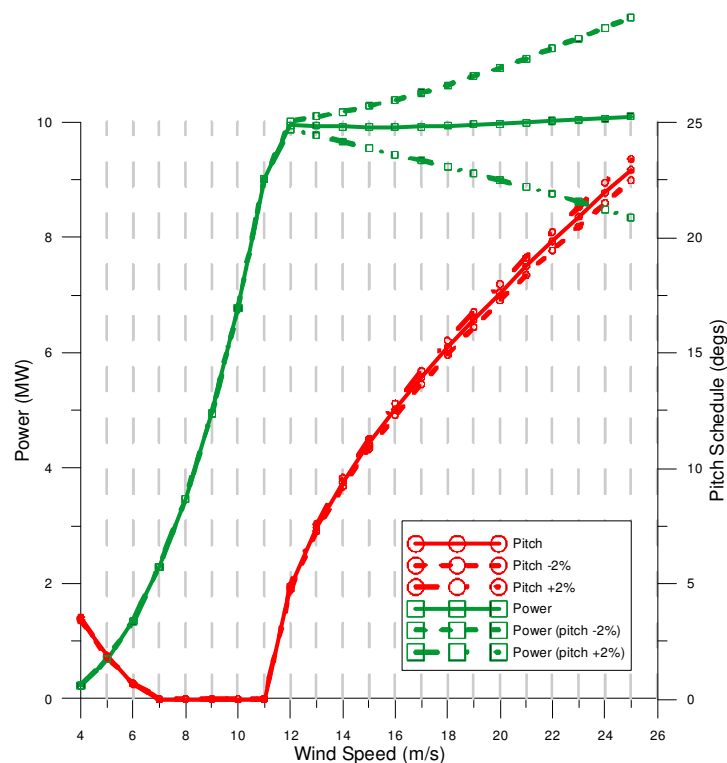


Figure 10. Power curve sensitivity to pitch angle

Figure 10 presents the sensitivity of the power curve to pitch variations at post rated wind speeds. The initial pitch schedule has been multiplied with 98% and 102% and the figure presents the power output variation to this $\pm 2\%$ change. It is seen that the power production sensitivity to the pitch setting is extremely high, especially at higher wind speeds. For this level of variation the response is nearly linear. We recall that in order to arrive at a flat post-rated power curve we already had to multiply the provided pitch schedule by 99%. If not, we were obtaining a dropping power curve (placed just in between the unlabelled and the +2% power curves of figure 10).

Blade Chord

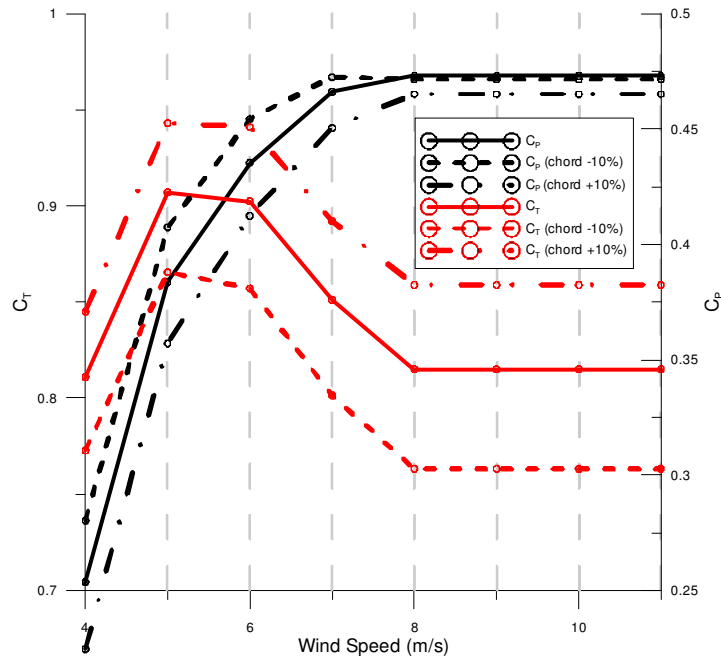


Figure 11. Power and thrust coefficients sensitivity to blade chord

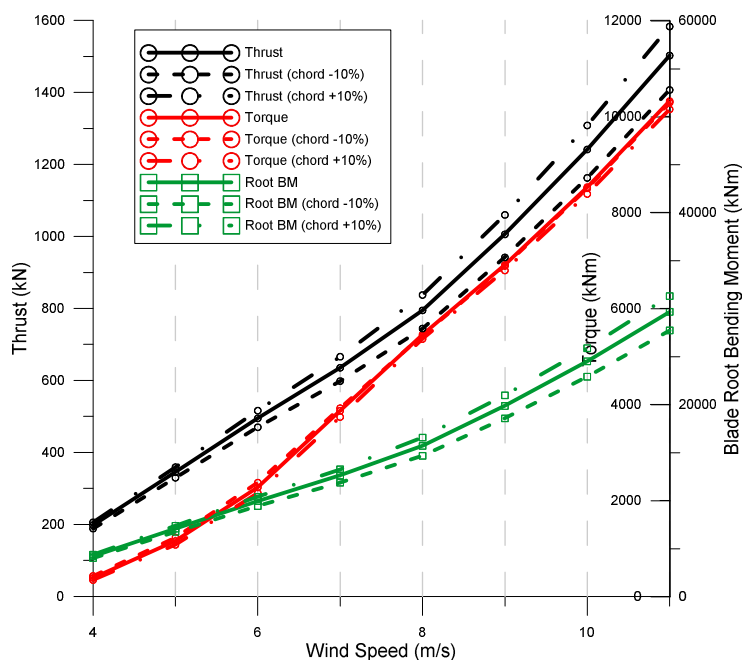


Figure 12. Torque, thrust and blade root bending moment sensitivity to blade chord

Figures 11 and 12 present the influence of $\pm 10\%$ variation of rotor solidity to the power coefficient, thrust coefficients and the rotor loads at below-rated wind speeds. The variation of the solidity has identical effect with that of a similar variation of the non-dimensional lift λ . Consequently the conclusions drawn from this investigation are also

applicable to the more general case in which the product of blade chord and the design lift coefficient is varying by $\pm 10\%$. From figure 11 it is seen that the C_{P_MAX} value is relatively insensitive to the Λ variation, especially when Λ gets lower values. The sensitivity of the thrust coefficient is much higher and its response is rather linear to the variation. Similar conclusions can be drawn from figure 12, this time for the dimensional torque, thrust and the blade root bending moment. The figure suggests that a 10% reduction of the blade chord of the initial design leads to a reduction of the maximum root bending moment from 30 000 to 28 000 kNm, without significantly affecting the rotor torque (and therefore the power production). This can be done either by reducing the chord by 10%, as long as the smaller blade sections can undertake the smaller load, or by reducing by 10% the design lift (using less cambered airfoils, for instance).

Airfoils' Performance

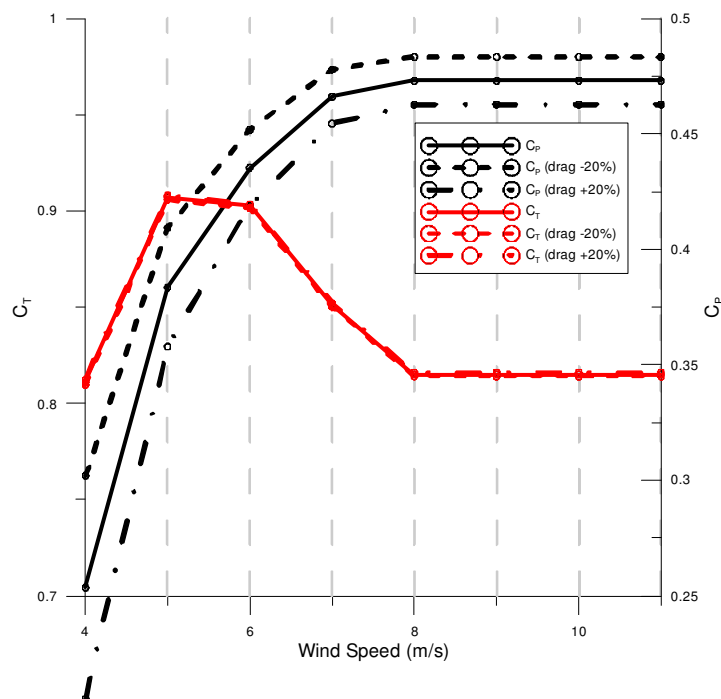


Figure 13. Power and thrust coefficients sensitivity to airfoils' drag

The next step is to investigate in a similar way the sensitivity of the power coefficient, thrust coefficients and the rotor loads to the airfoils performance characteristics. To do that we shall retain lift but vary $k = \max(C_L/C_D)$ by changing the drag coefficient by $\pm 20\%$. The results are presented in figures 13 and 14. This time, it is the thrust (and therefore the root bending moment) which is completely insensitive to the variation while there is a significant, rather linear, reaction of C_{P_MAX} (and therefore of power production).

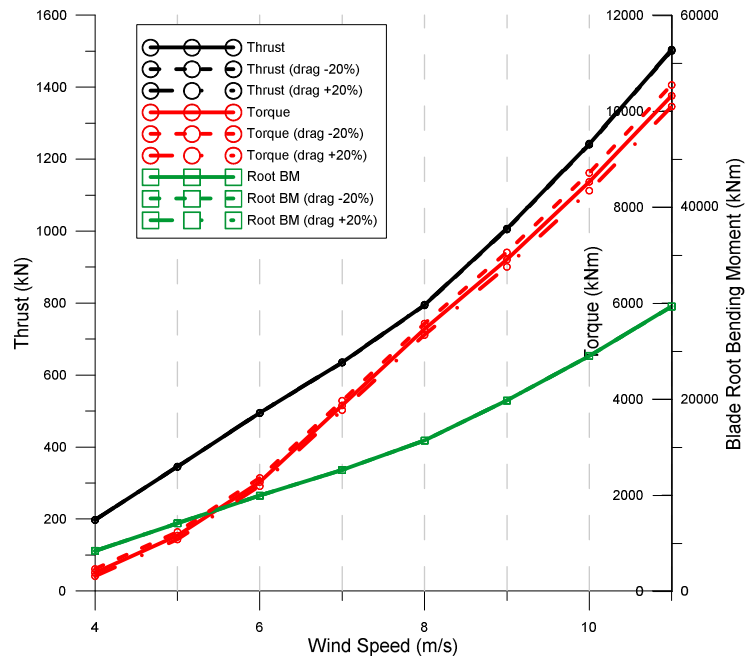


Figure 14. Torque, thrust and blade root bending moment sensitivity to airfoils' drag

STRUCTURAL PARAMETRIC ANALYSIS

The current section presents a preliminary analysis regarding the effect of mass and stiffness parameters on the natural frequencies of the InnWind.EU 10MW RWT blade [1]. Purpose of the analysis is to investigate the sensitivity of the blade dynamic response on structural modifications, as a preliminary check on the innovative structural solutions to be investigated within InnWind.EU.

Based on the structural data provided by DTU for the reference blade initially the blade structural parameters are reviewed aiming at identifying potential areas for improvement through innovative solutions proposed within WP2.

Blade structural properties

For the smooth operation of the wind turbine as a system, operational characteristics of the blade form also constraints of the blade structure. As presented in [6] these include the natural frequencies of the blade, especially the first flap and edge bending natural frequencies. For modern wind turbines (and larger blades) as a general rule of thumb the first natural frequency of the blade (in the flap direction) is close to $4p$ with p being the rotational frequency of the rotor, while the first natural frequency of the blade in the edge direction is close to $5.5p$, to comply with requirement of good first-frequency separation and avoid dynamic excitations affecting the overall operation of the wind turbine [7].

In Figure 15 the 1st natural frequency in the flap direction, normalized with the rotational speed of the relevant wind turbine, is presented for various blades. The DTU reference blade is shown with a filled mark quite close to $4p$ (rotational speed of the reference wind turbine 9.6rpm). For all cases presented, $3p$, an excitation frequency of the wind turbine is avoided.

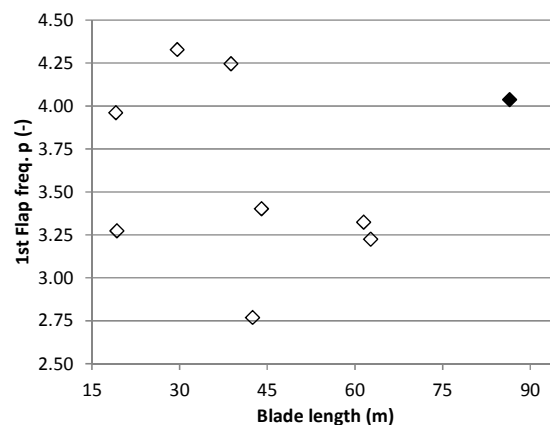


Figure 15. First frequency in flap direction for various blades with respect blade length

Similar in Figure 16 the normalized first natural frequency in the edge direction is presented for various blades. The result of the DTU reference blade is close to $6p$. Of course for the variable speed wind turbine a Campbell diagram is more appropriate to check the dynamic response, instead of the point simulation presented in here.

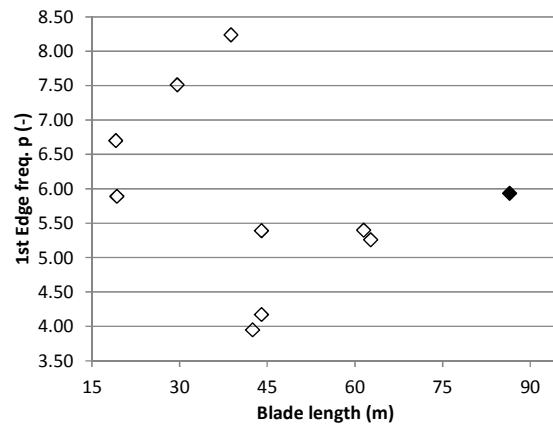


Figure 16. First frequency in edge direction for various blades with respect to blade length

Following [6], through an overview of the stiffness and mass properties of the blade, a preliminary verification of the blade behaviour against design constraints can be achieved. These design constraints include deflection, which is controlled through stiffness; buckling limitations, controlled through (local) stiffness and strength; the natural frequencies, as explained in the above; as well as in part extreme and variable load carrying capacity, controlled through stiffness and strength.

Regarding the mass and stiffness distribution along the blade length, some comments are possible when comparing the normalized stiffness values along the length for various blade sizes (see also [6]). Bending stiffness distribution along the blade is shown in Figure 17 and Figure 18 for the flap and edge direction, respectively, for various blade sizes. Both stiffness and position are normalized against the rotor radius, R . Stiffness data are normalized using the 4th power of the rotor radius, as suggested in [8]. The data for the 750kW are presented in [9], those of the 2.5MW wind turbine blades in [10], while those of the 5MW refer to the UPWIND reference blade [11]. Finally, the data for the 10MW blade are deduced from the structural data provided by DTU within the InnWind.EU project [1]. From Figures 17 & 18 it can be seen that the 10MW reference blade follows the stiffness in the outboard part of the blade of the multi-MW blades, while it is stiffer inboard.

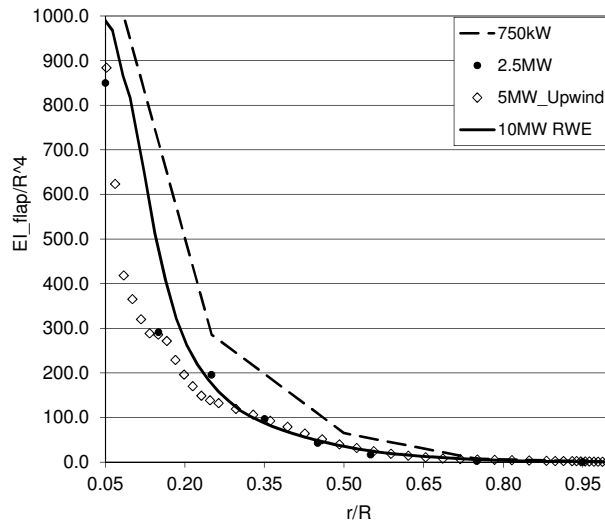


Figure 17. Stiffness distribution along the blade in flapwise direction for various blade sizes

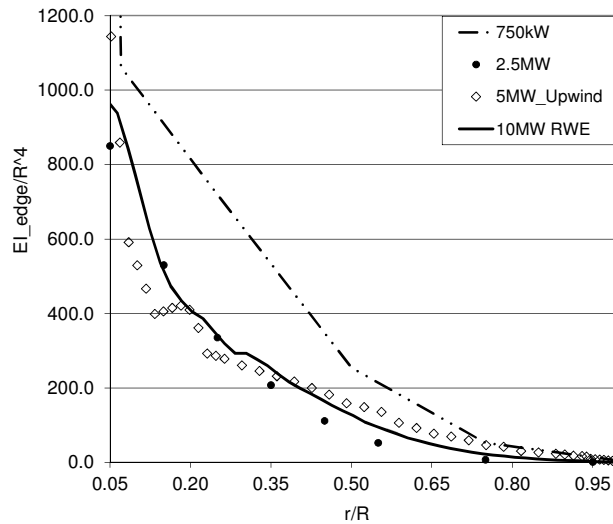


Figure 18. Stiffness distribution along the blade in edgewise direction for various blade sizes

An indicative distribution of the mass along the blade length is shown in Figure 19. The mass is normalized using the 2nd power of the rotor radius, as suggested in [8]. For cases included in the figure the presented stiffness and mass distribution data refer to preliminary blade designs and therefore most likely additional masses, which do not have a pronounced effect on the strength and stiffness of the blade (during the structural design) but are indispensable on the actual structure, such as the mass of the adhesive, the mass of the lightning protection system, etc., have not been included in the analysis. This additional mass is called “parasitic mass” in [9] and as indicated in that work, if this mass is not adjusted, then the results regarding mass estimations should be considered as a minimum. The reference 10MW DTU blade is quite lighter outboard, while following the mass trend inboard, again in comparison to the multi-MW blades. In the case of the 10MW DTU blade, nevertheless, it is stated that the data provided do not include the mass of the adhesive or other additional masses.

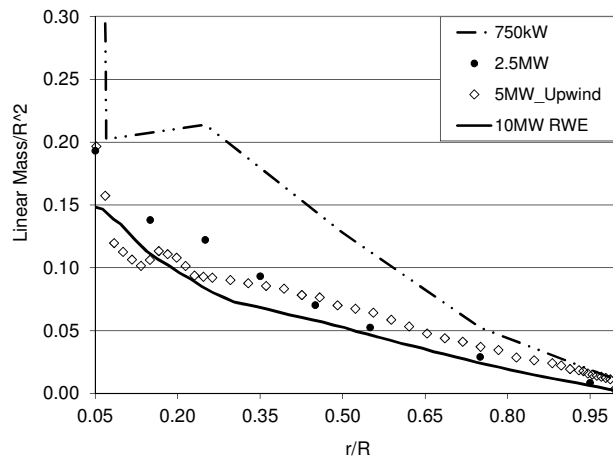


Figure 19. Normalized mass distribution along the blade for various blade sizes

Model Verification

Modelling of the blade structure was limited to beam elements exploiting the information provided by DTU [1] in tabular form. For the blade model 2-noded tapered beam elements were used with the commercial finite element software NISA II of EMRC, with following details:

- The blade model begins at station $R=2.8\text{m}$ and ends up at the station $R=89.166\text{m}$.
- The blade structure consists of 50 beam finite elements along its length and in total 306 degrees of freedom.
- The input needed for the beam formulation are the geometric properties of each section, i.e. the cross-sectional area, A ; the second order moments of inertia, I_{yy} , I_{zz} , and J and the material properties, i.e. the mass density, d , the moduli of elasticity and shear, E and G ; and the Poisson ratio, ν . These properties have been deduced by the data provided by DTU for each of the 51 cross-sections. A linear variation is assumed within the beam element.
- The offset of the elastic centre with respect to the pitch axis is accounted for by adjusting the eccentricity of the beam element's centre with respect to the global coordinate system.
- Eigenvalue analysis of the model is performed using a conventional subspace iteration technique.

A comparison of the eigenvalue analysis results in relation to the reference values provided by DTU is shown in Table 1. The differences from the reference values provided by DTU are less than $\pm 2\%$ with respect to the modal parameters. Both cases of the blade, namely the straight solution, as well as the pre-bend blade were modelled and results are presented in the table. As expected the difference in the dynamic response of those two cases is negligible (less than 0.5% in the natural frequency values).

Blade	Mass (kg)	Centre of Gravity (m)	Eigenfrequencies (Hz)		
			1 st Flap	1 st Edge	2 nd Flap
Reference	40814	26.008	0.646	0.949	1.792
Pre-bend	40481	26.213	0.632	0.962	1.818
Straight	40466	26.201	0.634	0.966	1.825

Table 1. Reference values of the RWT 10MW InnWind blade

Figure 20 shows the first eigenmode of the blade using the straight beam option. A small coupling between the flap and the edge direction is also depicted. Similar Figure 21 where the second eigenmode is presented.

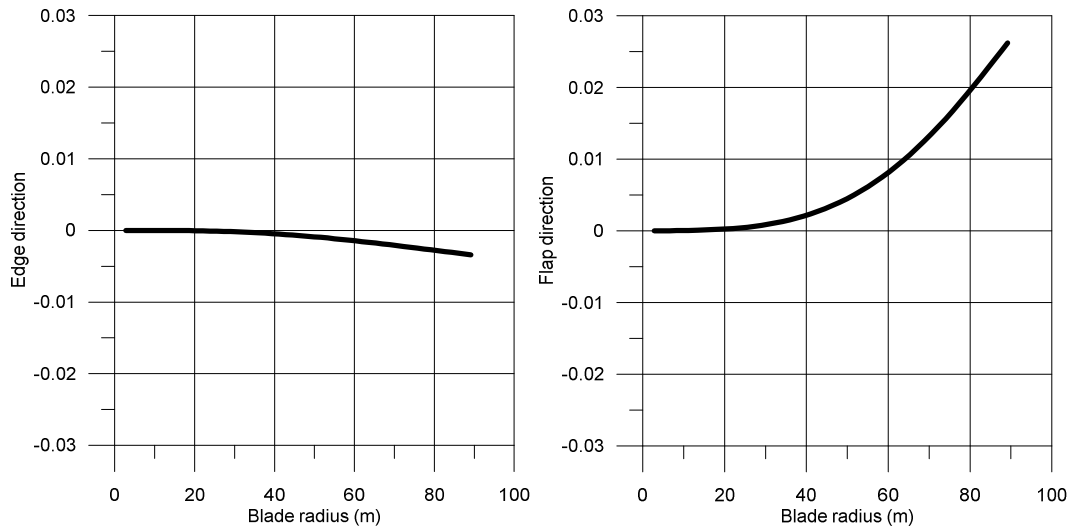


Figure 20. First blade eigenmode (0.634Hz) – straight blade model

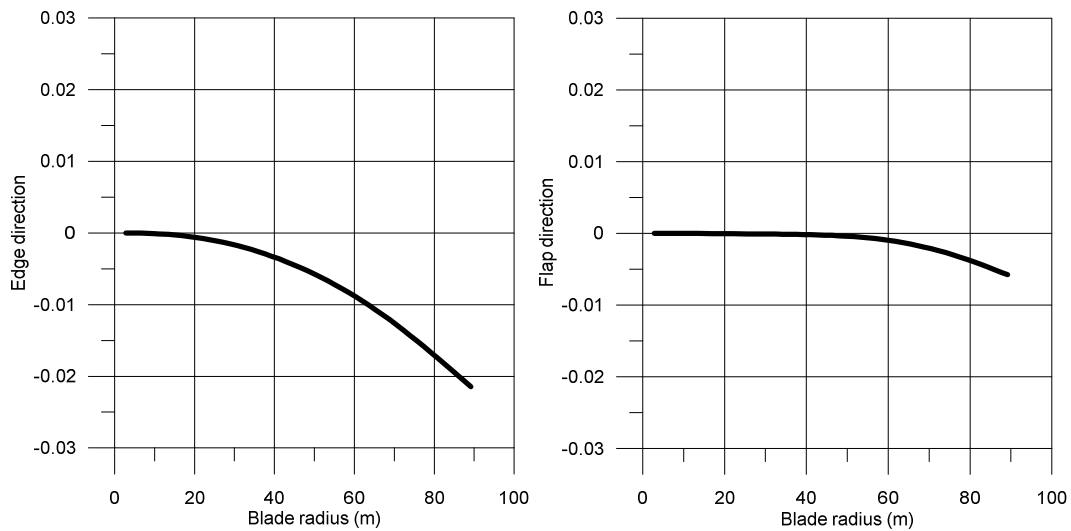


Figure 21. Second blade eigenmode (0.966Hz) – straight blade model

Therefore, it is concluded that the simplified blade model can be used for the parametric analysis with respect to dynamic properties of the blade.

Effect of mass increase on blade dynamic response

Based on previous comments a set of analysis cases were carried out in order to investigate the effect of the blade’s mass on the dynamic response of the blade. Only the mass increase has been considered in this analysis. Yet, it should be noted that it is possible that the results of the investigations within WP2 will indicate possibilities also of mass decrease. Nevertheless, since the “parasitic mass” will not be part of the investigations it is considered that the mass of the DTU reference blade represents a minimum.

For modelling the mass increase it is assumed that the additional mass follows the chord distribution along blade’s span (Figure 22). A set of five cases were applied, which corresponded to 2%, 4%, 6%, 8% and 10% increase of the blade’s total mass. Figure 22a shows the blade total mass increase, whereas Figure 22b presents the extra mass distribution along the blade’s cross-sections. The additional mass was modelled using mass elements along the blade length.

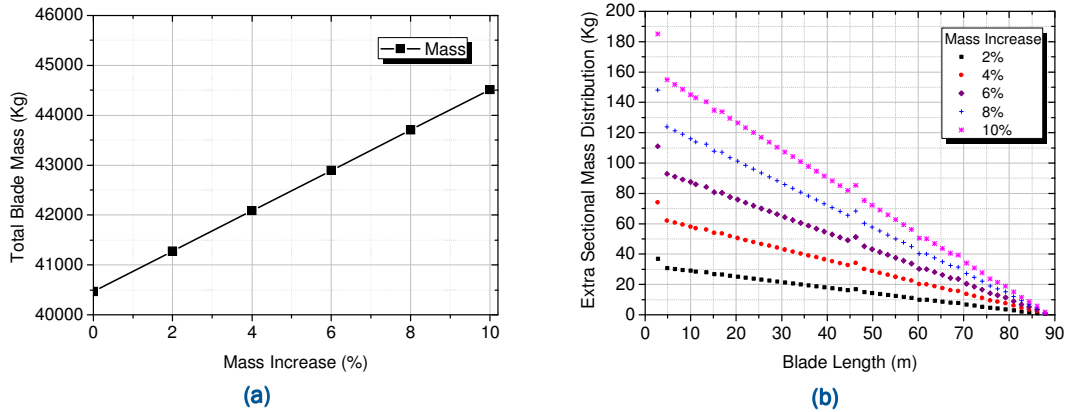


Figure 22. Blade mass increase: (a) Total blade mass; (b) Mass distribution along blade's span

The effect of mass increase was firstly quantified by predicting the natural frequencies of the blade. In detail, the first two flapwise and the first edgewise natural frequencies calculated are presented in Figure 23. The linear total mass increase gives out a respective linear decrease of structure's natural frequencies values, yet a 10% mass increase corresponds to less than 6% frequency decrease. The position of the blade's centre of gravity (C.G.) follows the same trend and is slightly (0.35m) transposed towards the blade's tip for the case of 10% blade mass increase. Had the mass increase been applied uniformly increasing the mass density of each section by e.g. 10%, the position of the centre of gravity would not be affected, while the frequency decrease would be less than 5%.

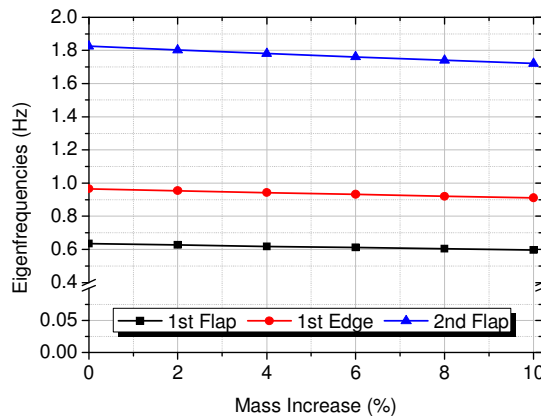


Figure 23. First three natural frequencies of the blade model for increasing mass values

With these assumptions, the frequencies of the blade normalized with the rotor rotational speed are approaching 3.7p in the flap direction and 5.7p in the edge under a 10% mass increase. The opposite behaviour, i.e. a frequency increase would have been attained in case of mass decrease.

Effect of stiffness increase on blade dynamic response

To investigate the effect of the stiffness on the dynamic response of the wind turbine blade stiffness increase was assumed. This falls in alignment with the work to be performed within WP2, regarding innovative structural solutions that lead to increased stiffness and/or mass reduction of the rotor blades. The stiffness increase was implemented in the blade model uniformly in two ways:

- Increasing the equivalent modulus of elasticity (per 5% or 10%) and
- Increasing the bending moments of inertia, I_{yy} and I_{zz}

The sensitivity of the blade against these two options was evaluated separately, since the elasticity modulus better represents the internal structural configuration and the materials, while the bending moments of inertia are closely related to geometric characteristics, e.g. the chord and thickness of the airfoil as well as the material thickness and less with location of potential shear webs. The sensitivity against the flapwise and the edgewise bending stiffness parameters was evaluated individually to highlight the effect of possible changes in specific geometric characteristics of the blade. For example the chord length of the airfoil is affecting the edgewise stiffness, while the thickness of the airfoil the corresponding stiffness in the flap direction.

Figure 24 to Figure 26 present the sensitivity of first three natural frequencies to blade stiffness increase. Results of the mass increase are included for reference.

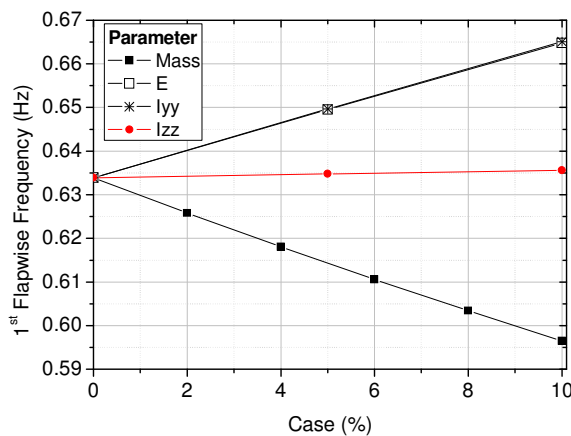


Figure 24. Variation of blade's 1st flapwise natural frequency

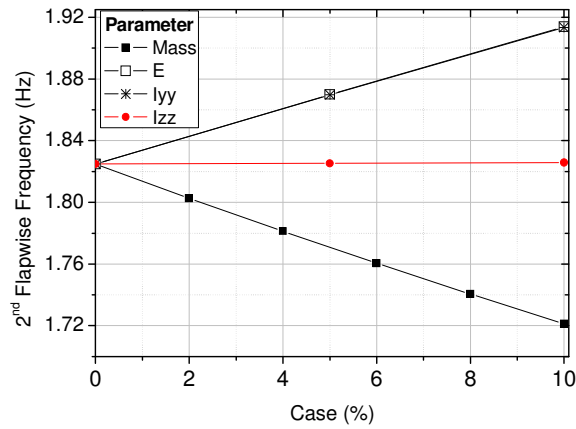


Figure 25. Variation of blade's 2nd flapwise natural frequency

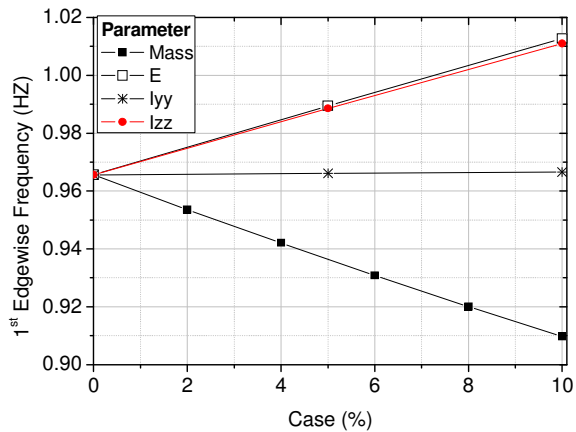


Figure 26. Variation of blade's 1st edgewise natural frequency

As it was expected, the higher values of equivalent elasticity modulus result in increased structure's stiffness and consequently in higher natural frequencies values. A 10% increase of the elasticity modulus results in about 5% increase of the natural frequencies.

Similar is the trend for the cases of the models with increased bending stiffness, while obviously an increase of I_{yy} affects only the eigenfrequencies in the flapwise direction, whereas the variation of I_{zz} has an effect only on the 1st edgewise natural frequency (Figure 26).

An increased stiffness of 10% (whether through the elasticity modulus or the bending moment of inertia) leads the first normalized frequencies of the blade to 4.2p in the flap direction and 6.3p in the edge, while the second flap frequencies is approaching 12p for the cases of increased elasticity modulus and I_{yy} .

CONCLUSIONS

The review performed for the aerodynamic part of the 10 MW DTU RWT confirms that the selections made and procedures followed for designing its blades are sound and the resulting outcome is representative of the current state of the art in pitch-variable speed rotor design. Results obtained from the sensitivity analysis of the reference blade in terms of its non-dimensional lift and design drag distribution indicate that this blade is adequate to form the basis for further investigations in aerodynamic design in the context of WP1 and WP2, pursuing innovations that can might increase performance in a cost effective way.

The review performed for the structural part of the 10MW DTU reference wind turbine blade indicate that the blade in its present form is well suited to be used within InnWind.EU as a reference of the current technological status (G/Ep). Furthermore, the sensitivity analysis with respect to the stiffness and the mass of the blade showed that the DTU reference blade is adequate to form the platform for structural innovations for very large offshore applications that will be performed within WP2.

REFERENCES

1. C. Bak, F. Zahle, R. Bitsche, T. Kim, A. Yde, L.C. Henriksen, P.B. Andersen, A. Natarajan, M.H. Hansen, "Design and performance of a 10 MW wind turbine", submitted to J. Wind Energy
2. V.A. Riziotis, P.K Chaviaropoulos and S.G. Voutsinas, "Development of a State-of-the-art Aeroelastic Simulator for Horizontal Axis Wind Turbines. Part 2: Aerodynamic Aspects and Applications", Journal Wind Engineering, Vol 20, No. 6, pp. 423-439, (1996)
3. V.A. Riziotis and S.G. Voutsinas, "Gast: A General Aerodynamic and Structural Prediction Tool for Wind Turbines", EWEC'97, Dublin, (1997)
4. DTU Pitch / VS schedule, Innwind.EU Internal site
5. Peter Jamieson, Innovation in Wind Turbine Design, A John Wiley & Sons, Ltd., Publication, ISBN 978-0-470-69981-2, 2011
6. D.J. Lekou, Scaling limits & costs regarding WT blades, UPWIND deliverable D3.4.3, 2010, <http://www.upwind.eu/publications/3-rotor-structure-and-materials.aspx> (last accessed 22/5/2013)
7. E.S. Politis, P. K. Chaviaropoulos, V. A. Riziotis, S. G. Voutsinas, I. Romero Sanz, Stability analysis of parked wind turbine blades, Scientific Proceeding of the EWEC 2009, pp. 59-63, 16-19 March 2009, Marseille, France
8. P.K. Chaviaropoulos, P.J. van Langen, P. Jamieson, Similarity rules for W/T up-scaling, UPWIND report, 2007
9. D. A. Griffin, WindPACT Turbine Design Scaling Studies Technical Area 1 – Composite Blades for 80- to 120-meter Rotor, NREL report, NREL/SR-500-29492, 2001
10. K.J. Jackson, M.D. Zuteck, C.P. van Dam, K.J. Standish, D. Berry, Innovative Design Approaches for Large Wind Turbine Blades Wind energy, Vol. 8, pp. 141-172, 2005
11. J. Jonkman, P. Johansen, C. Lindenburg, P. Chaviaropoulos, E. v/d Hooft, D. Witcher, B. Hendriks, P. van Langen, UPWIND Reference Wind Turbine, ver.9, 2009